ORIGINAL PAPER

Numerical Study on the Mechanical Behavior of Shotcrete Lining with Yielding Support in Large Deformation Tunnel

Kai Yang[1,2] · Qixiang Yan[1] · Zhendong Shi[1,2] · Chuan Zhang[1] · Shuqi Ma[1]

Abstract

The yielding support has proven to be one of the most effective measures to control the large deformation of the tunnel, as it could well stabilize tunnel support structure by releasing the deformation energy in the surrounding rock and exerting the self-supporting ability of the surrounding rock. To explore the damage mechanical behavior of shotcrete linings with yielding supports in large-deformation tunnels, an elastic–plastic damage model of concrete was developed, and a numerical method for simulating the yielding support based on the double-node beam element and interface element was proposed. Then, the influences of the position and resistance of the yielding element on the behaviors of shotcrete lining were analyzed and discussed. The results indicate that the position and resistance of the yielding element have a significant effect on the distribution of damage, principal stress, axial force, and bending moment of the lining. In the tunnel dominated by horizontal deformation, the yielding structure with constant resistance symmetrically arranged at the waist of the tunnel sidewall has the best yielding effect. The damage and maximum axial force are minimal, and the maximum bending moment is relatively large but lower than the maximum bending moment that the lining structure can bear. Assuming that the yielding element position stays the same, the maximum lining axial force rises with increasing yielding resistance, the maximum bending moment shows an initially upward and subsequently downward trend as the yielding resistance rises, and the maximum damage shows a trend of first declining and then growing as the yielding resistance rises. It is also found that the resistance of the yielding component should be controlled within a reasonable range, neither too small nor too large, for the lining to be in good working condition.

Highlights

- A new elastoplastic damage model was developed to describe the post-peak strain-softening behavior of concrete.
- A numerical realization approach for yielding support mechanical behavior was proposed.
- The mechanical behaviors of shotcrete lining with yielding support were numerically analyzed.

1 Introduction

A large amount of energy has been stored in the tunnel surrounding rock under high geo-stress conditions. The hardness of the surrounding rock determines its energy release rate, and therefore exhibits two distinctively different characteristics of deformation and failure. Disturbed by tunnel excavation operations, generally, the rapid release of energy occurs in hard rocks, which might lead to rock-burst disasters, while the slower release of energy occurs in soft rocks, inducing large-deformation disasters (Chen et al. 2020; Xiao

✉ Qixiang Yan
  yanqixiang@swjtu.edu.cn

1 Key Laboratory of Transportation Tunnel Engineering,
   Ministry of Education, Southwest Jiaotong University,
   Chengdu 610031, People's Republic of China

2 China Railway Construction Kunlun Investment Group Co.,
   LTD, Chengdu 610040, People's Republic of China

et al. 2021; Zhang et al. 2021). Between them, large-deformation disasters often cause the distortion of steel arches, the breakage of anchor rods, and the cracking and damage of sprayed concrete, which bring huge challenges to the design and construction of tunnels. Effective control of large-deformation disasters is essential to reduce the risk of the construction period and the difficulty of maintenance during the operation period (Bai et al. 2021; Cui et al. 2020; Wu et al. 2020). At present, there are three main support types for large deformation in soft rock tunnels, namely, heavy support method, multi-layer support method and yielding support method. The surrounding rock of large-deformation tunnels usually has significant time-dependent characteristics. The traditional heavy support system causes the stress in the supporting structure to increase, which cannot effectively solve the continuously increasing surrounding rock pressure. Moreover, the multi-layer support scheme method is neither not the best choice due to the immaturity of theoretical design and engineering construction. For example, reasonable layer thickness and construction timing of layered lining need further research and analysis. By comparison, the yielding support method, which allows the support structure to produce a certain displacement under the condition of maintaining a high support pressure to continuously release the energy in the surrounding rock, can make full of the performances of both surrounding rocks and supporting materials. Therefore, the yielding support method has been widely used in soft rock tunnels with large deformation.

So far, various materials and devices for yielding support have been proposed. Timber was the first support material with yielding characteristics, and then sliding steel arch was subsequently used in a wide range of applications (Podjadtke 2009). With a fast-increasing number of large-deformation tunnels, researchers have proposed various yielding devices and conducted a large number of support tests according to local conditions. For example, Schubert (1996) proposed the lining stress controllers widely used in the Galgenberg tunnel. Kovári (2005) proposed highly deformable concrete with incredible deformability by adding cement, steel fibers, and hollow glass particles. This concrete has been widely used in the Lötschberg Base tunnel and the St. Martin La Porte site access tunnel of the Lyon Turin Ferroviaire (Thut et al. 2006). Qiu et al. (2018) proposed a support resistant limiting damper (SRLD) made of metal buckling characteristics and applied to the Yangshan tunnel of the Haolebaoji–Ji'an Railway. These materials and structures promote the applications of yielding support technology in large-deformation tunnels.

Several studies have been carried out to investigate the support characteristics of yielding elements and their influences on the mechanical behavior of shotcrete lining through analytical solutions, field tests and numerical simulations. Wu et al. (2021) studied the analytical equations of the supporting characteristic curve of the circular tunnel lining with the circumferential yielding elements and thus improved the design method of yielding support. Tian et al. (2016) used a numerical simulation method to study the influence of the interface between the lining and the surrounding rock on the mechanical behavior of the yielding support structure. The concrete lining adopts the Mohr–Coulomb constitutive model, which might result in the overestimation of the bearing capacity of the damaged lining. Wu et al. (2018) proposed a new yielding support system that uses foamed concrete as both a cushion layer and a circumferential yielding structure, and investigated the deformation and stress of the lining by numerical simulation. Tian et al. (2018) used the connector element to simulate the mechanical characteristics of the yielding structure, and studied the influence of the yield stress of the yielding element on the mechanical behavior of the shotcrete lining. Lei and Zhao (2020) studied the mechanical properties of a metal buckling type yielding structure and analyzed the principle of circumferential yielding support from the perspective of energy transformation during tunnel excavation. Wang et al. (2016) studied the technical issues such as yielding support timing and yielding deformation amount based on the large deformation characteristics of the Dujiashan highway tunnel. From the above research, the yielding performance cannot be accurately reflected in these studies, or the lining material adopts an unreasonable constitutive model, such as the elastic model and Mohr–Coulomb model. It also lacks consideration of degradation of the shotcrete performance after lining failure. This study intends to use the finite difference method to investigate the mechanical behavior of shotcrete lining with yielding support in large-deformation tunnels, however, no built-in concrete constitutive model is available. Therefore, it is necessary to propose a suitable mechanical constitutive model for the shotcrete lining and accurately simulate the mechanical behavior of yielding element.

This study aims to investigate the effect of the yielding element on the internal force and failure behavior of the shotcrete lining. A new concrete elastoplastic damage model and a numerical realization scheme for the mechanical behavior of yielding support were proposed. The influences of the location and resistance of the yielding element on the damage mechanical behavior of the large-deformation tunnel lining were analyzed. Furthermore, the proper layout position and resistance of the yielding element were studied. The numerical research will be beneficial for gaining a better understanding of the interaction of shotcrete lining and rock for yielding supports.

2 The Damage Mechanics Model for Shotcrete Lining

A linear elastic constitutive model for concrete lining is frequently employed in the investigation of the mechanical behavior of tunnel construction, which is reasonable in the case of small deformations. However, if the tunnel experiences a large-deformation disaster, the employment of an elastoplastic model will overestimate the supporting effect of the lining, causing the structural design to become unreasonable. In the case of large deformation, the nonlinear mechanical behaviors of the concrete lining should be considered, requiring the development of a new concrete constitutive model. Concrete is an artificial composite material with significant changes in composition and complex mechanical properties. The difference in material ratio and pouring environment results in complex mechanical properties. Under the uniaxial compression and uniaxial tension, concrete exhibits a high degree of nonlinearity, as shown in Fig. 1. It shows that both curves under two loading conditions have rising and descending stages. The initial stage of the ascending stage of the compression curve can be regarded as the linear elastic behavior, and the ascending section near the peak and the curve after the peak show

obvious plastic characteristics. The area before the peak of the tension curve can be regarded as a linear elastic segment, and the curve after the peak shows the characteristic of plasticity decline. The descending rate under compression drops slower than that under tension, indicating that ductile deformation mainly occurs during compression, while brittle deformation is dominant during tension (Chen 2005).

The damage and failure modes and mechanisms of concrete under compression and tension are significantly different. Therefore, damage models can be established according to different loading modes: shear failure under compression and tensile failure under tension. The elastoplastic damage model of concrete is proposed by adding the damage variable to the Mohr–Coulomb model. The relationship between plastic shear strain κ_s and shear damage D_s is established for compression failure. For tension failure, the relationship between plastic tensile strain κ_t and tensile damage D_t is established.

2.1 Mechanical Equations of the Damage Model

The plastic shear damage model of concrete under compression can be divided into the pre-peak and post-peak damage stages. The damage in the pre-peak stage is defined by the decline in the secant modulus, while the

Fig. 1 Concrete test curves under monotonic loading (Guo and Shi 2003). **a** Stress–strain curve under compression; **b** Stress–displacement curve under tension
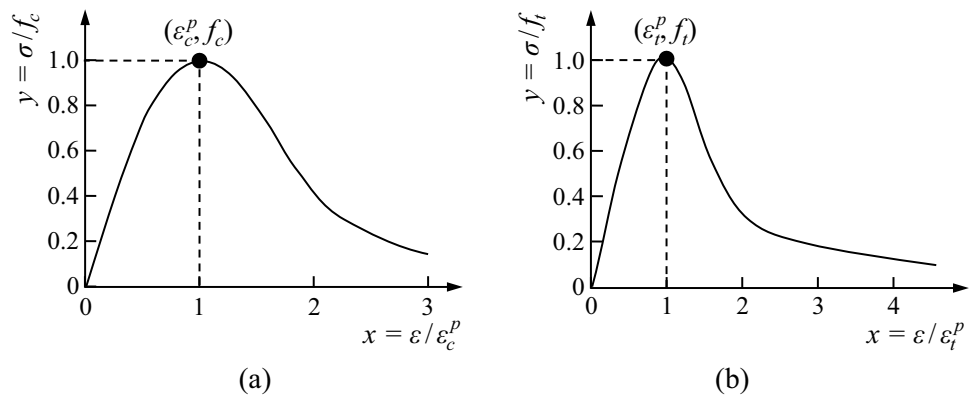
Fig. 2 The nonlinear behaviors of the damage model. **a** Shear damage; **b** Tensile damage
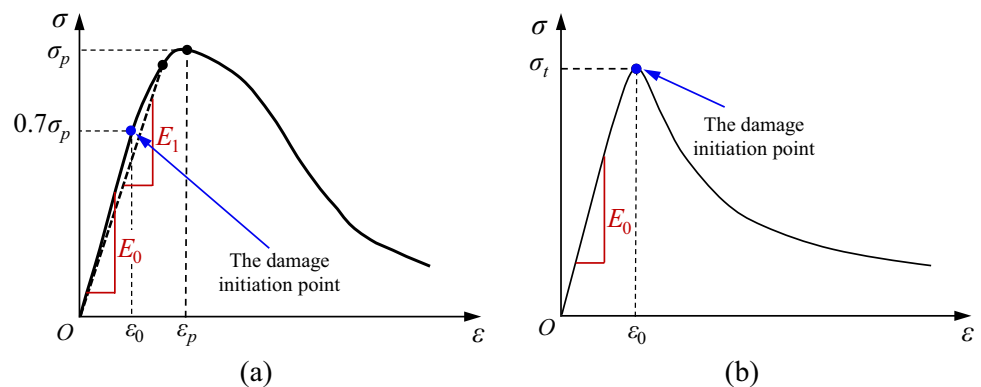
damage in the post-peak stage is defined by the decrease in stress, as shown in Fig. 2a.

At the pre-peak damage stage, the shear damage variable D_s is

$$D_s = 1 - \frac{E_1}{E_0} = 1 - \frac{\sigma}{E_0 \varepsilon} \tag{1}$$

where E_1 is the secant modulus, E_0 is the undamaged elastic modulus.

When the stress reaches its peak σ_p, the corresponding strain is ε_p. The damage variable associated with the peak stress is written as

$$D_p = 1 - \frac{\sigma_p}{E_0 \varepsilon_p} \tag{2}$$

The σ_p and ε_p of different concrete proportions are not equal, resulting in unequal D_p.

At the post-peak damage stage, the value of the damage variable continued to accumulate at the value D_p. The shear damage variable D_s can be expressed as

$$D_s = D_p + \left(1 - D_p\right)\left(1 - \frac{\sigma}{\sigma_p}\right) = 1 - \left(1 - D_p\right)\frac{\sigma}{\sigma_p} \tag{3}$$

The tensile damage behavior is assumed to be in an undamaged elastic condition until the tension reaches the tensile strength σ_t, at which point damage begins, as shown in Fig. 2b. The damage variable D_t can be expressed as

$$D_t = 1 - \frac{\sigma}{\sigma_t} \tag{4}$$

2.2 Three-Dimensional Form of the Damage Model

In the principal stress space, the expression of stress increment (Itasca 2012) expressed by strain increment is

$$\begin{aligned}
\Delta\sigma_1 &= \alpha_1 \Delta\varepsilon_1^e + \alpha_2\left(\Delta\varepsilon_2^e + \Delta\varepsilon_3^e\right) \\
\Delta\sigma_2 &= \alpha_1 \Delta\varepsilon_2^e + \alpha_2\left(\Delta\varepsilon_1^e + \Delta\varepsilon_3^e\right) \\
\Delta\sigma_3 &= \alpha_1 \Delta\varepsilon_3^e + \alpha_2\left(\Delta\varepsilon_1^e + \Delta\varepsilon_2^e\right)
\end{aligned} \tag{5}$$

where α_1 and α_2 are material constants defined in terms of the shear modulus G and bulk modulus K, as

$$\begin{cases}
\alpha_1 = (1 - D)\left(K + \frac{4}{3}G\right) \\
\alpha_2 = (1 - D)\left(K - \frac{2}{3}G\right)
\end{cases} \tag{6}$$

where $K = E/[3(1-2v)]$, $G = E/[2(1+v)]$. E is the elastic modulus, v Poisson's ratio.

Assuming that damage occurs in the post-peak stage under compression, the failure criterion for shear damage (Xu and Gutierrez 2021) is

$$f^s = \sigma_1 - \sigma_3 N_\phi + 2c\sqrt{N_\phi}(1 - D_s) \tag{7}$$

where $N_\phi = (1 + \sin\phi)/(1 - \sin\phi)$, c is the cohesive force, ϕ is the internal friction angle.

When the load reaches a specific peak strength ratio, the model enters the damage stage. Guo (1999) revealed that when the stress-to-peak strength ratio is between 0.3 and 0.8, concrete transitions from an elastic to a plastic state. The ratio is set at 0.7 in this study. Therefore, the failure criterion at the pre-peak stage is

$$f^s = \sigma_1 - \sigma_3 N_\phi + 2c\sqrt{N_\phi}(0.7 + 0.3D_s/D_p), \quad D_s \leq D_p \tag{8}$$

At the post-peak stage, the failure criterion is modified from Eq. (7) as

$$f^s = \sigma_1 - \sigma_3 N_\phi + 2c\sqrt{N_\phi}(1 - D_s)\Big/(1 - D_p), \quad D_s > D_p \tag{9}$$

The failure criterion for tensile damage (Xu and Gutierrez 2021) is

$$f^t = \sigma_3 - (1 - D_t)\sigma_t \tag{10}$$

The potential functions g^s and g^t define the shear and tensile plastic flow, respectively. The mathematical expression (Itasca 2012) can be expressed as

$$\begin{cases}
g^s = \sigma_1 - \sigma_3 N_\psi \\
g^t = -\sigma_3
\end{cases} \tag{11}$$

where Ψ is the dilation angle, $N_\psi = (1 + \sin\Psi)/(1 - \sin\Psi)$.

It is necessary to judge whether it is a shear failure or tensile failure after the element reaches the plastic state. It can be judged according to the function $h(\sigma_1, \sigma_3) = 0$ in the principal stress space, and the mathematical expression is

$$\begin{aligned}
h &= \sigma_3 - \sigma^t + a^P(\sigma_1 - \sigma^P) \\
a^P &= \sqrt{1 + N_\phi^2} + N_\phi \\
\sigma^P &= \sigma^t N_\phi - 2c\sqrt{N_\phi}
\end{aligned} \tag{12}$$

The following formula can determine the failure type of the element

$$\begin{cases}
f^s \leq 0, & h \leq 0 \text{ shear damage} \\
f^t \leq 0, & h > 0 \text{ tensile damage}
\end{cases} \tag{13}$$

When shear damage occurs, the formula of principal stress is

$$\sigma_1^N = \sigma_1^I - \lambda^s(\alpha_1 - \alpha_2 N_\psi)$$
$$\sigma_2^N = \sigma_2^I - \lambda^s\alpha_2(1 - N_\psi) \tag{14}$$
$$\sigma_3^N = \sigma_3^I - \lambda^s(-\alpha_1 N_\psi + \alpha_2)$$

$$\lambda^s = \frac{f^s(\sigma_1^I, \sigma_3^I)}{(\alpha_1 - \alpha_2 N_\psi) + (-\alpha_1 N_\psi + \alpha_2)N_\phi} \tag{15}$$

When tensile damage occurs, the formula of principal stress is

$$\sigma_1^N = \sigma_1^I - \lambda^t\alpha_2$$
$$\sigma_2^N = \sigma_2^I - \lambda^t\alpha_2 \tag{16}$$
$$\sigma_3^N = \sigma_3^I - \lambda^t\alpha_1$$

$$\lambda^t = \frac{\sigma_3^I - \sigma^t}{\alpha_1} \tag{17}$$

The damage mechanical behaviors of concrete can be achieved by establishing a mapping relationship between plastic strain and damage variable as

$$\begin{cases} D_s = f(\kappa_s) \\ D_t = f(\kappa_t) \end{cases} \tag{18}$$

The internal mapping relationships can be determined by back-analysis of the concrete post-failure behaviors.

The plastic shear strain κ_s is defined as the sum of plastic shear strain increment $\Delta\kappa_s$, given as

$$\kappa_s = \sum \Delta\kappa_s = \sum \sqrt{\frac{(\Delta\varepsilon_1^{ps} - \Delta\varepsilon_m^{ps})^2 + (\Delta\varepsilon_m^{ps})^2 + (\Delta\varepsilon_3^{ps} - \Delta\varepsilon_m^{ps})^2}{2}} \tag{19}$$

$$\Delta\varepsilon_m^{ps} = \frac{\Delta\varepsilon_1^{ps} + \Delta\varepsilon_3^{ps}}{3} \tag{20}$$

$$\Delta\varepsilon_1^{ps} = \lambda^s \tag{21}$$

$$\Delta\varepsilon_3^{ps} = -\lambda^s N_\psi \tag{22}$$

The plastic tensile strain κ_t is defined as the sum of plastic tensile strain increment $\Delta\kappa_t$, given as

$$\kappa_t = \sum \Delta\kappa_t = \sum \left| \Delta\varepsilon_3^{pt} \right| \tag{23}$$

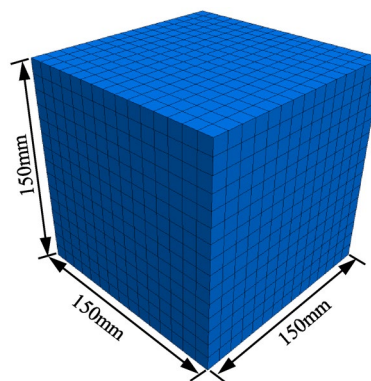$$\Delta\varepsilon_3^{pt} = \lambda^t \tag{24}$$

Fig. 3 The dimension of the numerical model

2.3 Model Validation

According to the three-dimensional form of the concrete damage model, the model is established through secondary development in the C++ language environment and further compiled into a dynamic-link library file. The custom constitutive model is registered for user call using the commands *config cppudm* and *model load*. Based on the stress–strain curve of the C25 concrete in Code for the design of concrete structures (Ministry of Construction of the People's Republic of China 2002), the proposed damage model was verified by the uniaxial compression and tensile tests. A cubic numerical model was established with a side length of 150 mm, which consists of 3375 elements, as shown in Fig. 3. The bottom of the specimen was fixed and compressed downward from the top. The vertical displacement of the top center and the top surface reaction force during the loading process are recorded. The mechanical parameters of concrete are shown in Table 1. The damage parameters are shown in Table 2.

The numerical result of the stress–strain curve of the damage model under monotonic load was obtained. Under uniaxial compression, the simulated stress–strain curve shows an elastic stress state before 70% of the peak stress, as shown in Fig. 4a. After the load exceeds 70% of the peak value, the concrete enters a shear damage state, and the curve slope gradually decreases till the stress reaches to its peak value. Immediately after the peak stress, the curve shows an apparent strain-softening behavior. At this time, the peak stress obtained by the numerical simulation is very close to the standard value. Therefore, the proposed elastoplastic damage model of concrete can well describe the elastic section, plastic section and strain-softening stage of concrete under compression. Under uniaxial tension, the simulated stress–strain curve also shows obvious elasticity

Table 1 Basic mechanical parameters of concrete

Material	E (GPa)	Poisson's ratio υ	γ (kN m^{-3})	c (MPa)	ϕ (°)	Compressive strength (MPa)	Tensile strength (MPa)
Concrete	28	0.2	22	3.0	50	16.7	1.78

before the peak stress and strain-softening behavior at the post-peak stage, as shown in Fig. 4b. The curve is in good agreement with the curve in the Code for Design of Concrete Structures (Ministry of Construction of the People's Republic of China 2002), and the developed damage model can effectively reflect the mechanical behavior of concrete under uniaxial tension.

3 Mechanical Characteristics and Numerical Modeling of Yielding Support

3.1 Mechanical Characteristics of Yielding Support

The yielding support is mainly used to relieve pressure in the radial and/or circumferential direction of the tunnel. In the radial direction, constant resistance large-deformation bolt (cable) is mainly used to achieve yielding behavior (Tao et al. 2017; Wang et al. 2021). However, it is necessary to install some special yielding members in the lining to reduce deformation pressure in the radial direction and the internal force of the lining in the circumferential direction. At present, yielding members are divided into metal buckling yielding devices, structural sliding yielding devices, and devices made of high deformable concrete or foamed concrete. Metal buckling yielding devices include columnar, honeycomb, baffle and circular ring shapes, etc. (Lei and Zhao 2020; Qiu et al. 2018; Radončić et al. 2009). The structural sliding-type yielding device mainly includes the retractable steel arch and the constant resistance large-deformation bolt. Among these yielding members, the common circumferential yielding support system includes the retractable steel arch combined with high deformable concrete, the retractable steel arch combined with a deformation slot, and the retractable steel arch combined with a metal buckling yielding device, as shown in Fig. 5. In the following, the numerical simulation method will be employed to explore the mechanical behaviors of support system with retractable steel arch and the high deformable concrete element.

The stress–strain or load–displacement relationship of the yielding structure is obtained by axial compression testing. For example, the mechanical response of high deformable concrete elements is shown in Fig. 6a. It shows that the concrete maintains a relatively constant axial stress until

Table 2 Damage parameters of concrete

In compression		In tension	
κ_s ($\times 10^{-3}$)	D_s	κ_t ($\times 10^{-3}$)	D_t
0	0	0	0
0.06	0.01	0.42	0.55
0.20	0.02	1.02	0.75
0.45	0.03	3.6	0.99
1.20	0.11	/	/
3.00	0.40	/	/
4.50	0.70	/	/
7.00	0.99	/	/

the strain increases to about 40%. The high deformable concrete is composed of a mixture of cement, sand, hollow glass particles, steel fibers and additives, along with suitable steel reinforcement (Thut et al. 2006), which gives the material the ability to withstand large deformation without failure. By adding high deformable concrete elements, the tunnel shotcrete lining can deform along with the steel arch without being damaged, which increases the resistance of the supporting system. The mechanical response of the yielding structure can be obtained by simplifying the yielding characteristics of high deformable concrete element, as shown in Fig. 6b. It shows that the yielding stress σ_y (yielding resistance F_y) and the ultimate strain ε_{lim} (the ultimate yielding displacement s_{lim}) describe the mechanical behavior of the yielding structure. The yielding structure installed in the tunnel lining is simultaneously subjected to the circumferential pressure of the lining and the surrounding rock pressure. The surrounding rock pressure is generally distributed in the range of 0.4 ~ 1 MPa, while the circumferential pressure of the lining is much larger than the surrounding rock pressure (Guan 1993). The stress state of the yielded structure is approximately considered as a uniaxial compression state, similar to the loading path of high deformable concrete element in compression test. The reasonable yielding resistance F_y ensures that the surrounding rock is always in a controllable state without large deformation. A certain amount of circumferential deformation occurs in the lining structure, and the energy accumulated in the surrounding rock is gradually released. When the circumferential deformation of the lining reaches

Fig. 4 Validation of the damage model. a Uniaxial compression; b Uniaxial tension

(a)

(b)

(a)   (b)   (c)
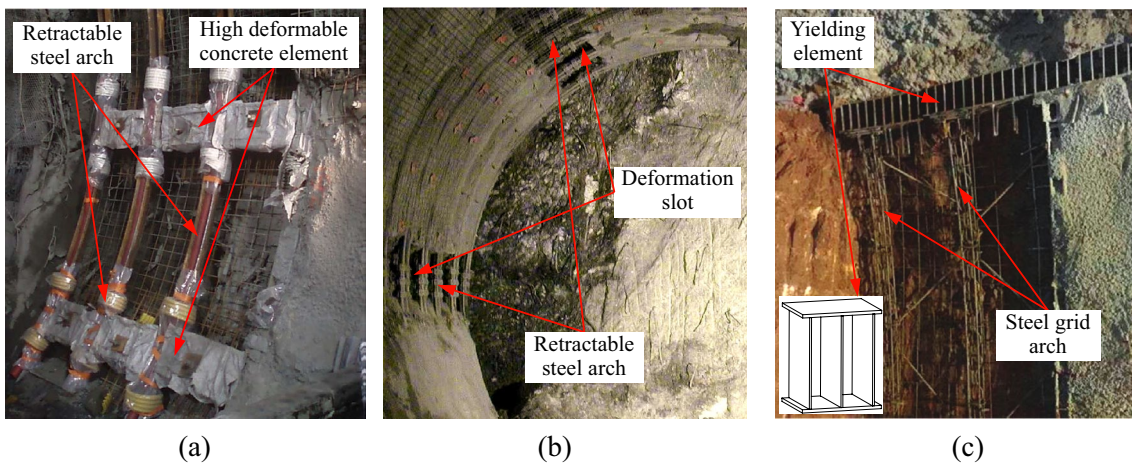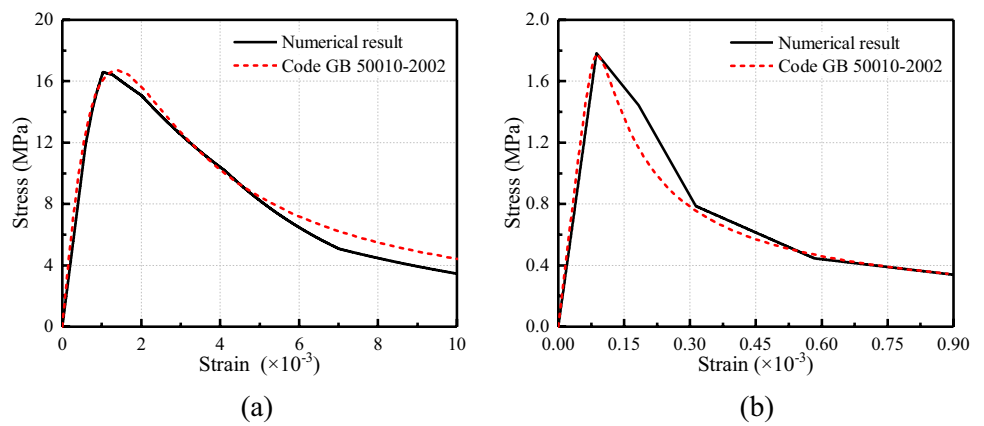
Fig. 5 Typical combination of yielding support. a Retractable steel arch combined with the high deformable concrete element (Barla et al. 2010); b Retractable steel arch combined with deformation slot (Fabbri 2004); c Steel grid arch combined with yielding element (Deng et al. 2020)

Fig. 6 Stress–strain characteristics of yielding element. a Test result (Kovári 2009); b Idealized curve

(a)   (b)
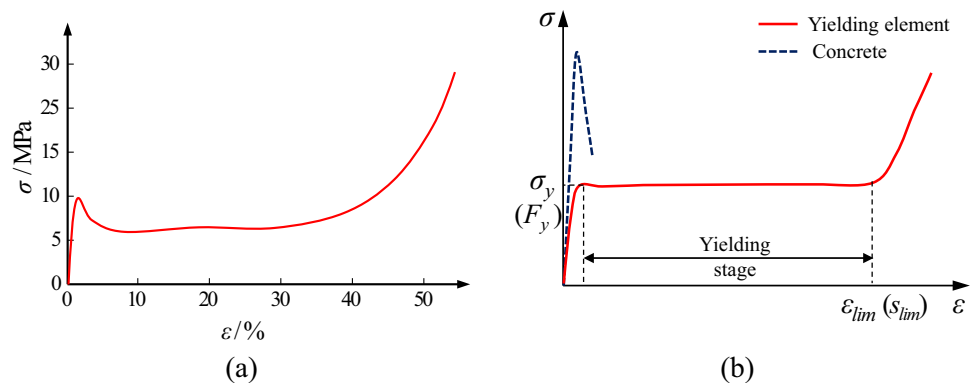
the ultimate yielding displacement s_{lim}, the axial force in the lining increases again. Therefore, a reasonable yielding resistance F_y ensures that the stress in the lining is lower than the compressive strength of the concrete, so that the lining is in a good service state without cracking.
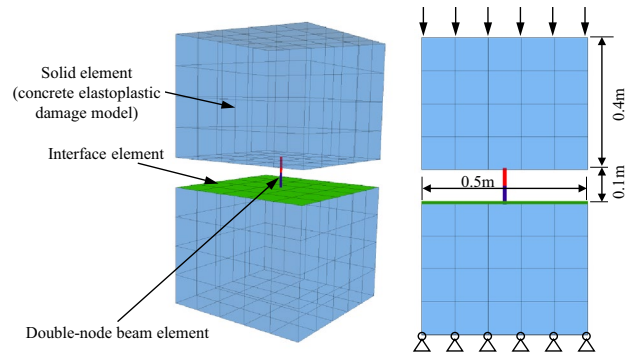
3.2 Numerical Modeling of Yielding Support

The beam element is a commonly used linear elastic structural element. Potential yielding behavior can be realized by creating double nodes at the deformation position, adding a
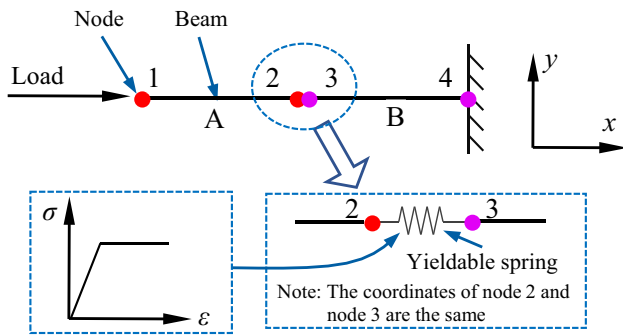
Fig. 7 The diagram of the double-node method to realize the yielding behavior

Fig. 8 Numerical model for validation of yielding behavior

node-to-node link between these nodes, and then specifying appropriate link attachment conditions. The principle of the double-node beam element to realize the yielding support is illustrated in Fig. 7. The *x*-axis is directed from node 1 to node 2, the *y*-axis and *z*-axis are arbitrarily oriented in the beam cross-sectional plane. Node 2 of beam element A and node 3 of beam element B have the same coordinates but different node numbers, so no force or moment is transmitted between the two nodes. To transfer force and moment between nodes, different types of links need to be set up. In this study, a yielding spring with ideal elastic–plastic behavior is set between node 2 and node 3 along the axis of the beam element. The rest of the directions are set rigid, that is, the *x*-direction is deformable, the *y*-direction and the *z*-direction are set rigid, and the rotational components of the *x*, *y*, and *z* axes are set rigid. The two-node method allows relative translation and/or rotation of adjacent beam elements, which is suitable for calculating the large strain and post-failure performance of the structure (Itasca 2012). The mechanical behavior of a yielding spring is controlled by two parameters, including the yielding strength and stiffness, but not by strain. Hence, the method cannot control the amount of deformation. This problem can be remedied by setting the interface element on the contact surface to

characterize the yielding displacement. In this way, the mesh does not penetrate after the deformation exceeds the limit, and the axial force in the yielding structure is transmitted to the element on the other side through the interface element. Therefore, a simulation method of yielding support is proposed, that is, the double-node beam element simulates the yielding behavior, and the interface element is set to simulate the mechanical behavior after the contact surface is closed.

3.3 Numerical Validation of Yielding Behavior

To validate the correctness of the yielding behavior simulation scheme, a numerical model is established, as shown in Fig. 8. The node-to-zone links are automatically established when the beam nodes are inside the solid elements. These links store the zone and an interpolation location within the zone to allow the transfer of forces and velocities between the nodes and the zones (Itasca 2012). The bottom of the model was fixed, and a downward displacement boundary with 103 mm was applied to the top of the model. A yielding spring was set between the beam element nodes with the same coordinates, and the yielding load of the spring was set to 1000 kN. During the numerical calculation, the axial force of the beam element, the displacement and load

Fig. 9 Mechanical behaviors of the numerical model. **a** The axial force–displacement curve of beam element; **b** The load–displacement curve of the yielding structure

(a)   (b)
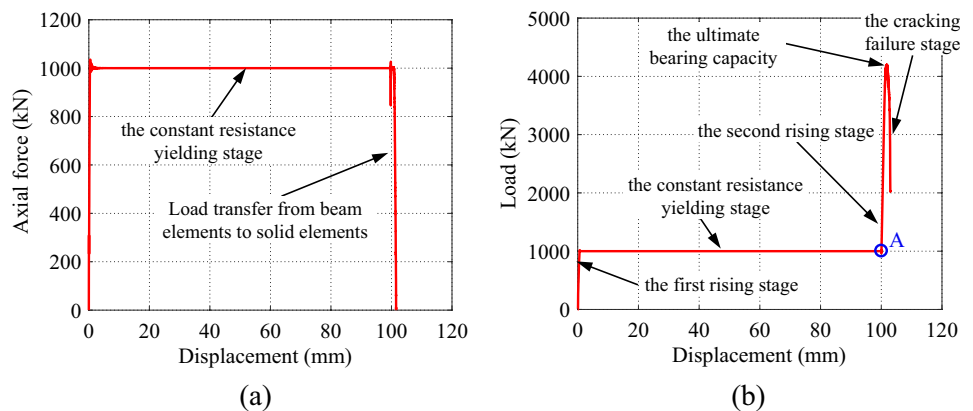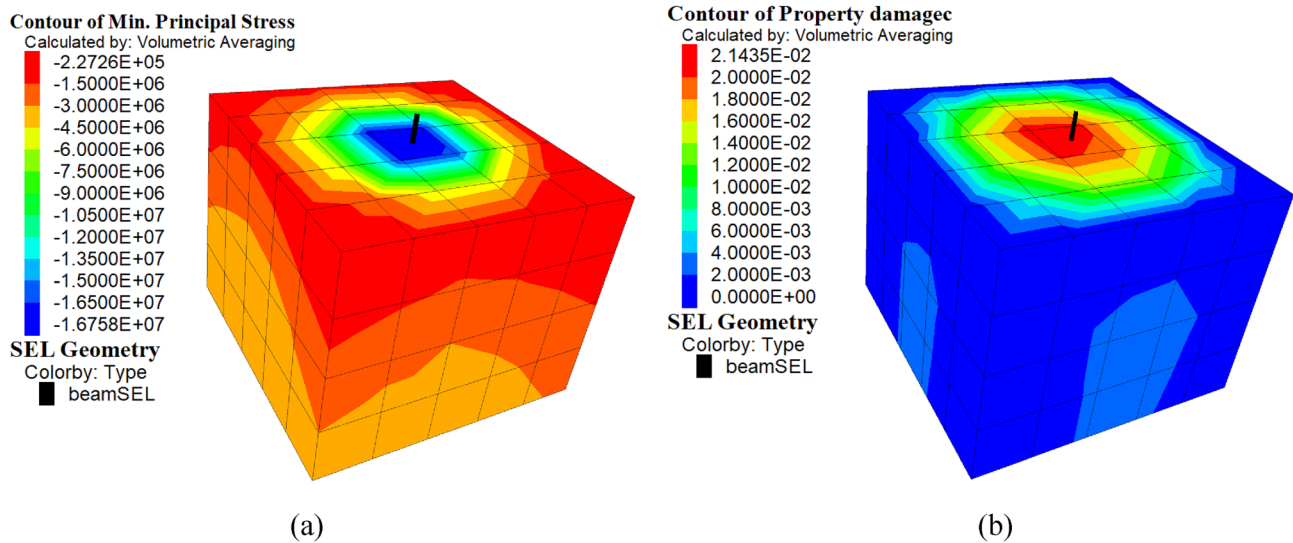
Fig. 10 Numerical results. **a** Principal stress distribution at the moment of contact surface closure; **b** Damage distribution at the moment of contact surface closure

at the top of the model were recorded simultaneously. Figure 9a shows the relationship between the axial force and displacement of the beam element. The axial force in the constant resistance yielding section is set to 1000 kN. When the applied displacement reaches 100 mm, the load in the beam element is gradually transferred to the lining due to the closed interface, and the axial force decreases rapidly. The load–displacement curve of the entire yielding structure is shown in Fig. 9b. The curve can be divided into four stages: the first rising stage, the constant resistance yielding stage, the second rising stage and the cracking failure stage. There is a linear elastic relationship between load and displacement in the first stage. When the yielding load of the spring reaches 1000 kN, the beam element begins to yield and bear a constant load. When the contact surface is closed (point A), the curve enters the second rising stage, and the load gradually increases as the loading process proceeds. When the ultimate bearing capacity of the structure is reached, the concrete is rapidly damaged and cracked, resulting in a quick drop of the curve. Figure 10a, b show the distribution of principal stress and damage at different loading stages, respectively. The results show that stress concentration occurs at the connection between the beam element and the solid element, resulting in the local damage of the model. To solve this problem, beam elements are set at the solid element nodes on both sides of the contact surface. In this way, the stress is transmitted by the multiple beam elements, which significantly reduces the degree of stress concentration. Therefore, the mechanical behavior

of the yielding structure can be reasonably simulated using the double-node beam element combined with the contact element.

4 Influence of Yielding Support on the Mechanical Behavior of Shotcrete Lining in Large Deformation Tunnel

The numerical analysis is based on the conditions of the Zongsi tunnel, located in Xiaozhongdian town, Yunnan Province, China. It is a crucial engineering project along the railway from Lijiang to Shangri-La. The tunnel is located at the southeastern edge of the Qinghai-Tibet Plateau and the middle section of the Hengduan Mountains. It is a well-known seismic belt in West Yunnan in China, with developed geological structures in the region. The tunnel is a single-track railway tunnel with a length of 2205 m and a maximum overburden of 190 m. The tunnel is approximately elliptical in cross-section, with a height of 996 mm and a width of 685 mm. It was investigated during the tunnel construction that the tunnel mainly passed through carbonaceous shale with poor integrity. The rock mass has low strength and presents squeezing deformation characteristics. The deformation of the tunnel was underestimated in the early construction stage. The tunnel horizontal convergence is much larger than the vault settlement. The maximum vault settlement and horizontal convergence are 328.7 mm and 738.9 mm, respectively.
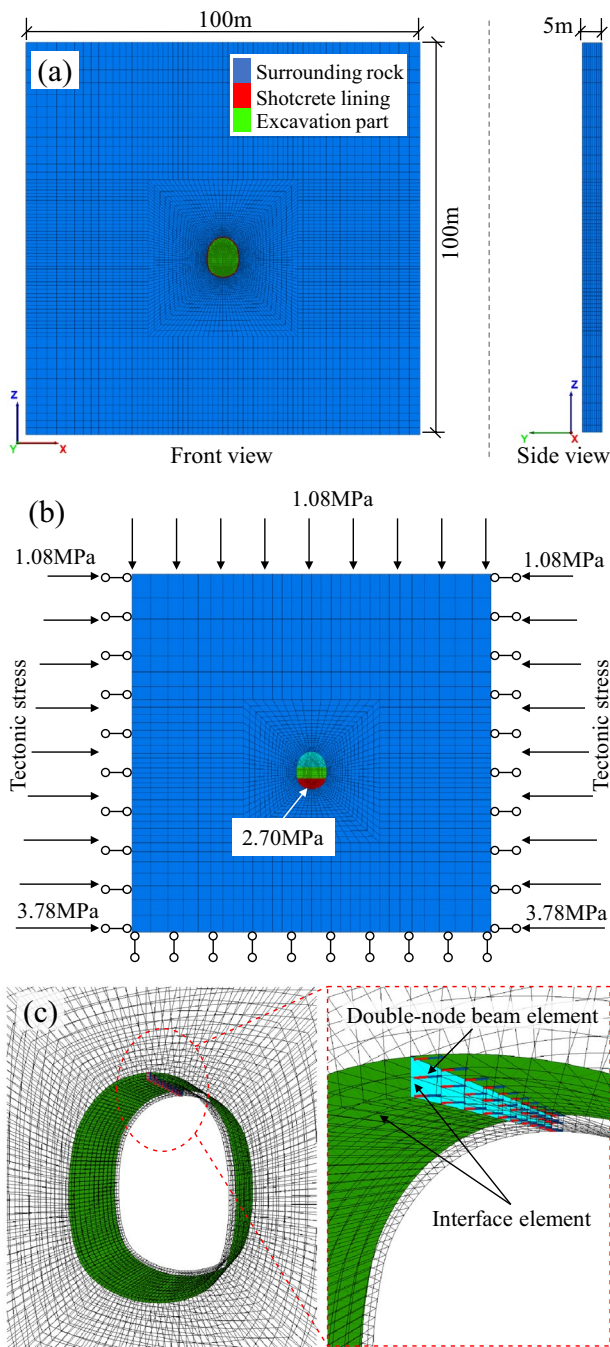
Fig. 11 Numerical model of yielding support. **a** model dimension; **b** model boundary conditions; **c** double-node element and interface element

The large deformation might cause unreasonable support methods and insufficient bearing capacity of the support structure, further leading to twisted steel frames, cracked linings, and serious primary lining invasion into tunnel

contour. In addition, the excavation heading face and initial support are very likely to collapse. The in-situ strength test of carbonaceous shale was carried out at the DK126 + 777 section of the Zongsi tunnel. The results show that the cohesion and internal friction angle of the surrounding rock were 0.221 MPa and 15.1°, respectively. The strength of the surrounding rock can be estimated to be 0.573 MPa based on the theory of (Hoek and Brown 1997). When the tunnel burial depth is 100 m and the unit weight of the surrounding rock is 27 kN/m^{-3}, the vertical geo-stress is about 2.7 MPa. The strength–stress ratio (Tao 1987) of the tunnel surrounding rock is 0.21. According to the Code for Design of Railway Tunnel (National Railway Administration of China 2016), when the strength–stress ratio is less than 4, the geo-stress is considered to be in an extremely high condition. Considering that the mileage of tunnels with a buried depth of more than 100 m accounts for more than 74%, the Zongsi Tunnel is judged as a high-stress soft rock tunnel, which is prone to large squeezing deformation disasters during construction.

### 4.1 Numerical Model of Yielding Support for Large Deformation Tunnel

In large-deformation tunnels, sliding can occur between the lining and the surrounding rock. The interface element, which is defined by three nodes (Itasca 2012), is used to simulate the sliding effect. Moreover, the three-dimensional model is used instead of the plane strain model. Figure 11a shows the numerical model used to analyze the mechanical behavior of yielding support in a large-deformation tunnel. The dimension of the model is 100 m in vertical and horizontal directions and 5 m in tunnel axial direction. The thickness of the shotcrete lining is set at 270 mm. Given that the buried depth of the tunnel is 100 m, and the unit weight of the surrounding rock is 27 kN m^{-3}. The lateral pressure

Table 3 Parameters of surrounding rock and supporting structure

Material	E (Gpa)	υ	γ (kN·m^{-3})	c (MPa)	ϕ (°)
Surrounding rock	0.08	0.35	27	0.22	15
Steel arch	210	0.3	79	–	–

Table 4 Creep parameters of surrounding rock

| Creep parameter	G^m (MPa)	η^m (MPa.d)	G^k (MPa)	η^k (MPa.d)
Value	41.3	349.5	16.6	15.8

Fig. 12 Layout of yielding elements
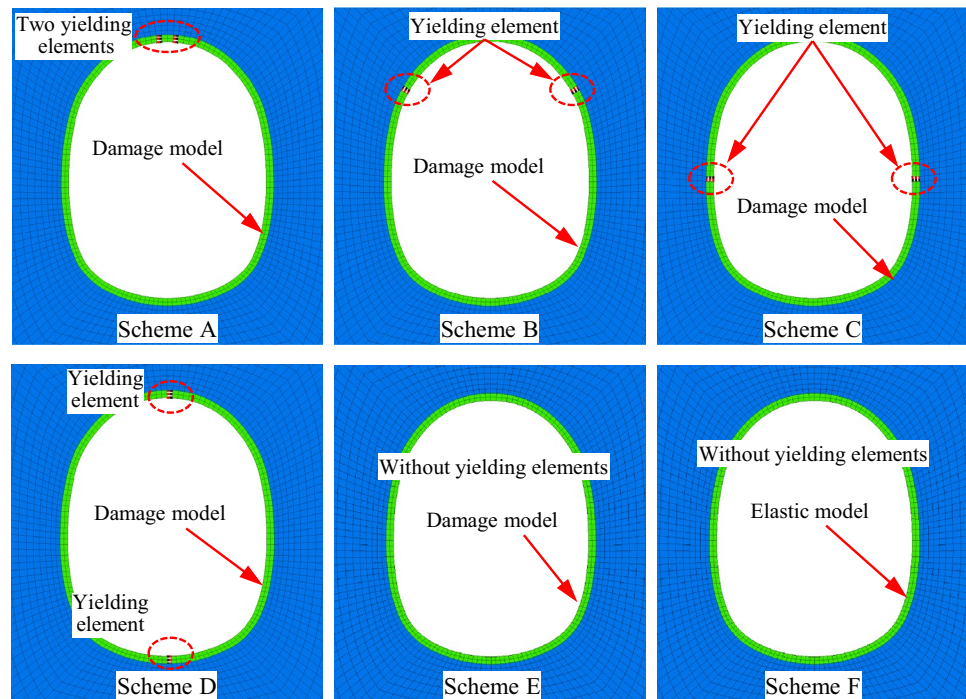
coefficient of the tunnel is 1, which is obtained from the on-site monitoring data. So, the horizontal stress and vertical stress at the tunnel body are 2.7 MPa. The boundary conditions applied to the model are shown in Fig. 11b. A stress of 1.08 MPa is applied on the model top surface to simulate the gravity stress generated by a rock layer with a thickness of 40 m. Displacement boundary conditions are used for the other five surfaces, that is, the normal displacements of the front, rear, left, right and bottom surfaces are fixed. At the same time, a tectonic stress that increases with depth is applied to the model. The yielding structure is jointly simulated by the double-node beam and the interface elements, as shown in Fig. 11c. The interface element is provided at the location of the yielding element to ensure that the axial force is transmitted after the lining is closed in the circumferential direction. At the same time, the interface element is also arranged between the surrounding rock and the shotcrete lining so that it can slide between the surrounding rock and the shotcrete lining. The cohesion of the interface element is set to 65 kPa and the internal friction angle is set to 30°. In the simulation analysis, the influence of bolt support and excavation by the bench cut method is ignored, and the effect of the steel arch is equivalent to the concrete. The surrounding rock and the lining are solid elements. The CVISC creep model and the developed concrete elastoplastic damage model were used for the surrounding rock and shotcrete lining, respectively. The strength grade of concrete is set to C25, the compressive strength is 16.7 MPa, and the tensile strength is 1.78 MPa. The surrounding rock, shotcrete and steel arch parameters are listed in Tables 1, 2, 3 and 4.

## 4.2 Position of Yielding Element

To prove that the lining damage can be reduced after setting yielding elements, and to study the influence of the position of the yielding elements on the mechanical behavior of the shotcrete lining, four schemes with yielding elements and two schemes without yielding members are proposed, as shown in Fig. 12. Among them, the constitutive model of the lining in Schemes A to E is the developed damage model, while the lining of Scheme F uses the elastic model. In each scheme, two yielding elements are arranged, and the deformation capacity of each yielding element is 200 mm. The resistance of the yielding element is set to 1800 kN, that is, the resistance provided by a yielding element per meter in the strike direction is 1800 kN. In this study, the yielding resistance is defined as the resistance provided by the yielding structure in the lining with a length of 1 m in the tunnel direction. Similarly, the axial force and bending moment of the lining in the following text are defined as the axial force and bending moment in the lining with a length of 1 m.
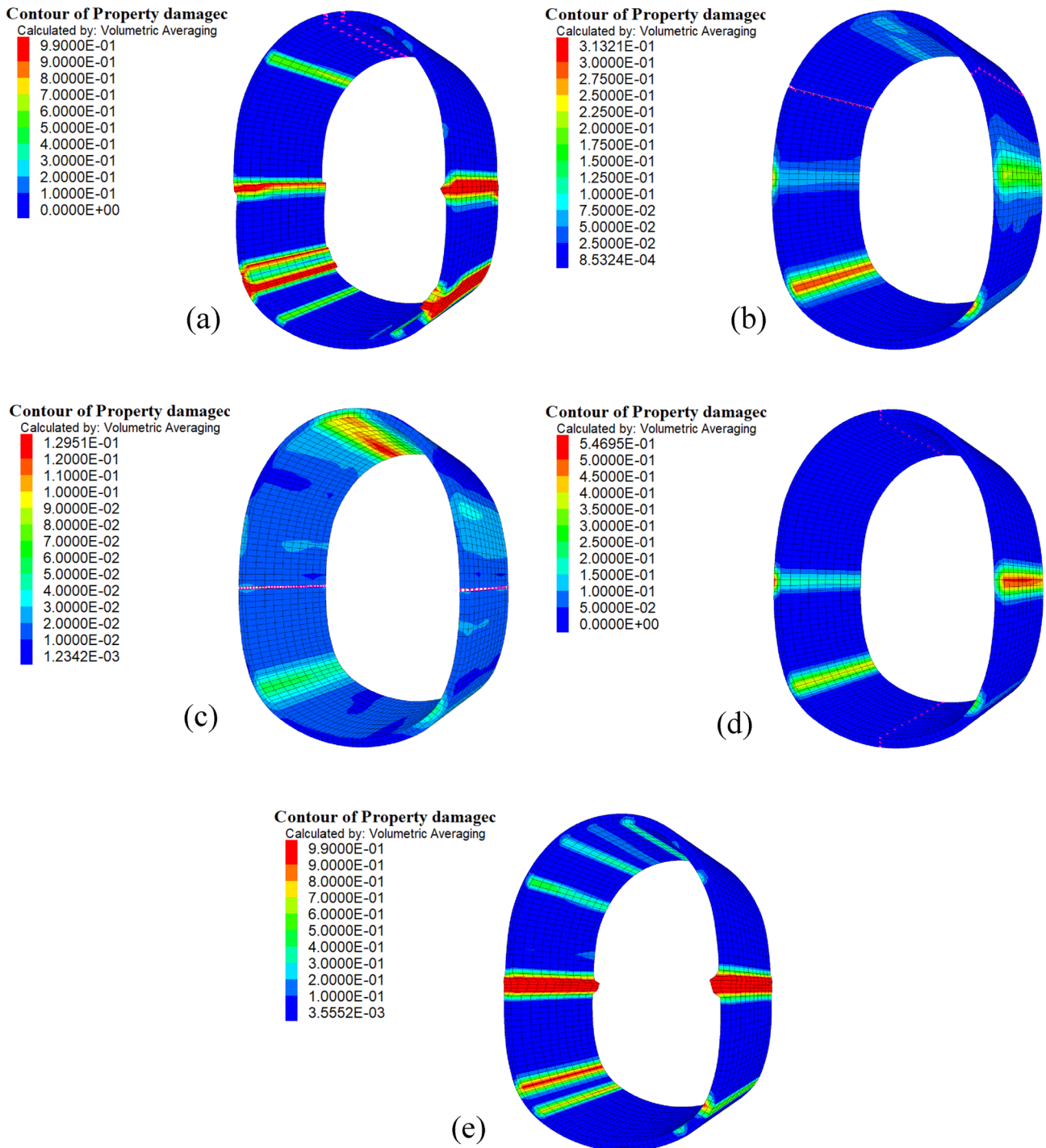
Fig. 13 Effect of yielding element position on lining damage. **a** Scheme A; **b** Scheme B; **c** Scheme C; **d** Scheme D; **e** Scheme E

The lining damage distribution characteristics of different schemes are shown in Fig. 13. Generally, these concrete lining sections with a damage degree over 0.9 can be regarded as the existence of cracking failure (Zhang et al. 2018). In scheme A, a penetration area with damage greater than 0.9 is formed at the waist and foot of the tunnel wall, indicating
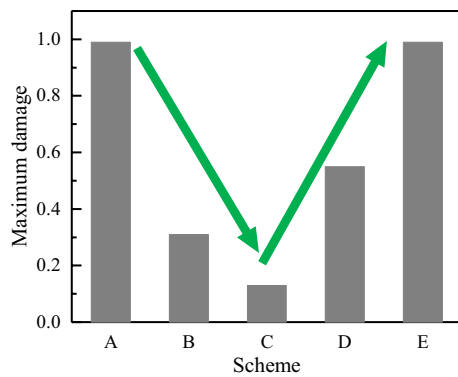
Fig. 14 Maximum damage of lining under different schemes

that the lining has almost completely lost its bearing capacity. In scheme B, the lining damage at the vault, the waist of the wall and the foot of the tunnel wall is high, and the maximum value is about 0.31. The damage at the vault and the foot of the tunnel wall is more significant in scheme C, and the vault has the highest lining damage with a value of 0.13. In scheme D, the damage is highest at the waist of tunnel wall, followed by the foot of tunnel wall, and the maximum damage value in the lining is approximately 0.55. Because there is no yielding member in scheme E, the lining forms a penetration area with damage greater than 0.9 at the waist of tunnel wall. Scheme F is not damaged due to the elastic model of the lining. The maximum damage of the lining in various schemes is shown in Fig. 14. It demonstrates that the lining damage in scheme C is the smallest. The yielding structure can significantly reduce the damage value and range in the lining, while also ensuring that the supporting structure can withstand large deformation without becoming unstable.

Figure 15 depicts the minimum principal stress distribution in the lining, which reflects the compressive stress distribution characteristics. The maximum stress in Scheme A is approximately 3.6 MPa due to stress release caused by lining failure. The maximum stress in the lining in Schemes B, C, and D is 13.2, 13.8, and 13.3 MPa, respectively, all of which are less than the compressive strength of concrete of 16.7 MPa. The stress at the vault and invert of scheme B is high. Scheme C has the highest stress at the arch foot, followed by the vault. The arch waist and wall foot are particularly stressed in Scheme D. The lining stress is high at the tunnel invert in Scheme E, and the maximum value is only 5.0 MPa because the lining has been damaged. The maximum compressive stress in the lining in Scheme F reaches 27.5 MPa, which is significantly higher than the compressive

capacity of concrete. As a result, the yielding member installation efficiently minimizes the stress in the lining, and the different installation positions change the stress distribution in the lining.

Figure 16 shows the axial force distribution of the tunnel lining. Due to the lining damage in scheme A, the axial force value is low, with a maximum value of less than 500 kN. In Scheme B, the axial force increases gradually from the vault, the waist, the sidewall to the invert of the tunnel. The axial force at the sidewall is very low in scheme C, whereas it is high at the arch and the invert of the tunnel. The yielding structure in scheme D is positioned at the vault and invert of the tunnel, so the axial force close to these two components is minimal. The failure of the lining in Scheme E results in a small axial force value. The axial force value in Scheme F is roughly twice that of Schemes B, C, and D. The yielding structure significantly reduces the axial force in the lining, and the cracked lining loses bearing capacity, so the axial force is low. Figure 17 depicts the bending moment distribution of the tunnel lining. Due to lining failure, Schemes A and E have small bending moments. The bending moment is positive at the sidewall of the tunnel and negative at the position of the arch and the foot of the wall in Scheme F using the elastic lining model. The maximum positive and negative bending moments values are about 228.9 kN m and −244.9 kN m, respectively. In Schemes B and C, the range of positive bending moments in the lining decreases, and the bending moment near the tunnel invert becomes negative. In Scheme D, almost all of the bending moments distributed in the lining are negative. Furthermore, the bending moment values in schemes B, C, and D are significantly lower than those in scheme F.

Figure 18a depicts the greatest axial force in the lining. Because of the lining damage in Schemes A and E, the axial force is low. In comparison to the elastic lining model, schemes B, C, and D using the yielding structure greatly reduce the axial force in the lining, with scheme C having the best yielding effect. Figure 18b shows the maximum bending moment in the lining. Similarly, the bending moments in Schemes A and E are small due to lining failure. Schemes B, C, and D can all greatly lower the bending moment in the lining, with Scheme D being the minimum. The yielding elements, when compared to scheme F, can reduce both the axial force of the lining and the bending moment. The lining can deform in a circumferential direction due to the presence of the yielding element. The circumferential deformation releases a part of the deformation energy of the surrounding rock, which not only reduces the axial force of the lining, but also reduces the surrounding rock pressure on the lining. As
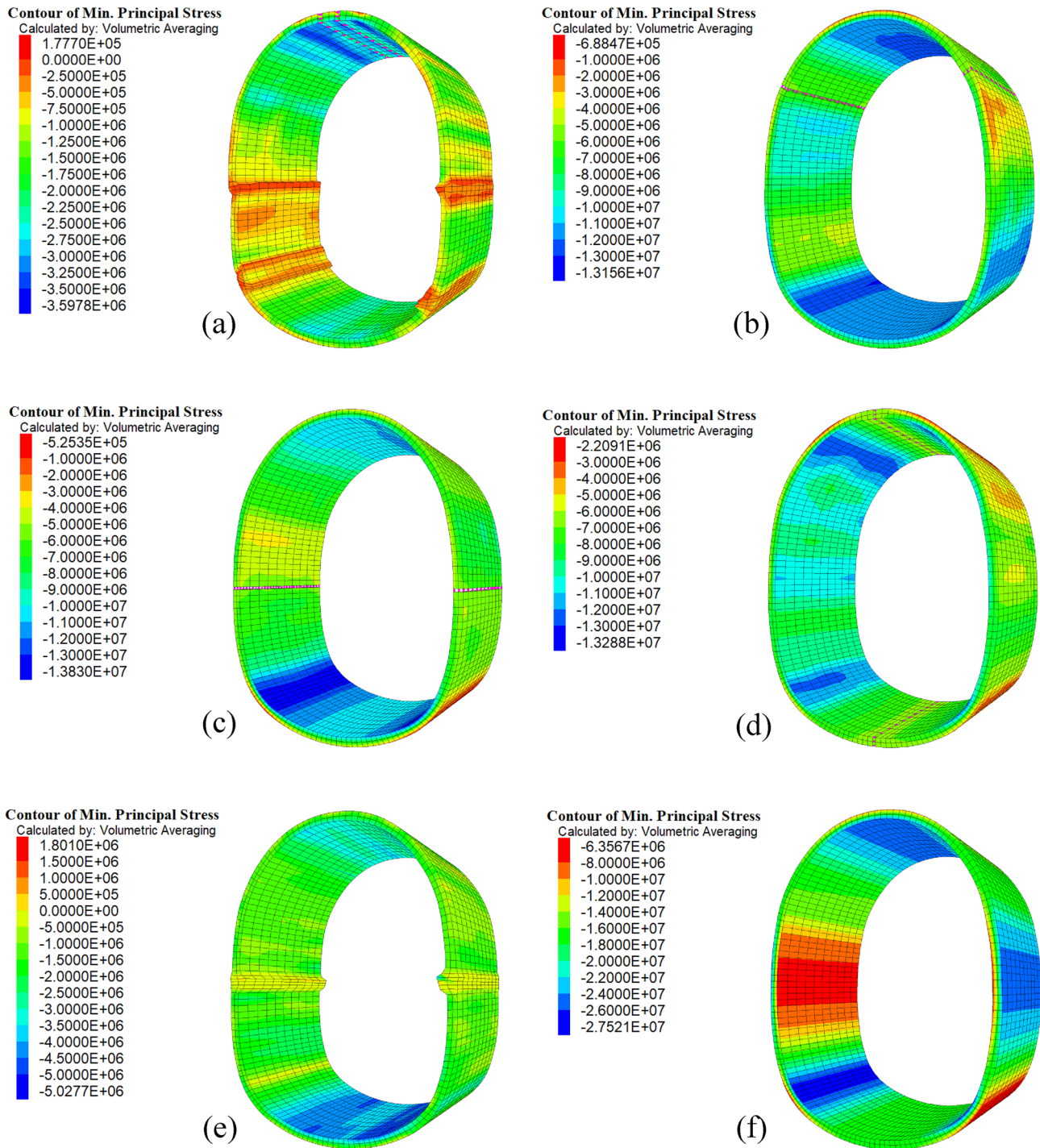
Fig. 15 Effect of yielding element position on the minimum principal stress (Unit: Pa). **a** Scheme A; **b** Scheme B; **c** Scheme C; **d** Scheme D; **e** Scheme E; **f** Scheme F

a result, Scheme C with the yielding structure symmetrically placed at the waist of the tunnel sidewall has the best support effect in terms of minimizing lining damage. In this scheme,

the axial force of the lining is minimal, and the bending moment is relatively large but less than the ultimate bending moment of the lining structure.
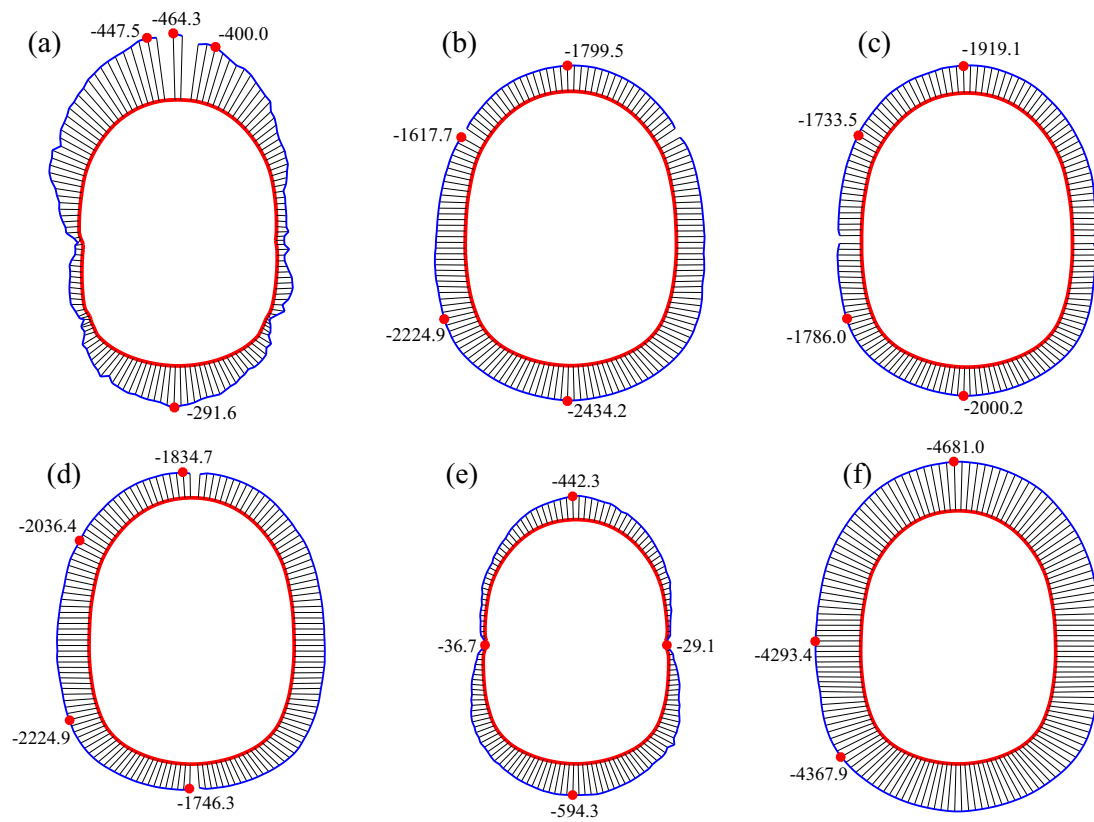
Fig. 16 Effect of yielding element position on axial force (Unit: kN). **a** Scheme A; **b** Scheme B; **c** Scheme C; **d** Scheme D; **e** Scheme E; **f** Scheme F

4.3 Resistance of Yielding Element

The yielding member was installed at the waist on both sides of the tunnel to investigate the influence of the yielding element resistance on the mechanical behaviors of the lining. Each set of yielding elements has a 200 mm deformation capacity. The distribution of damage, stress, axial force, and bending moment of the lining were analyzed for the six cases where the resistance of the yielding element is 1500, 1800, 2100, 2400, 2700, and 3000 kN.

The damage distribution characteristics of the lining under various resistance of the yielding member are shown in Fig. 19. When the yielding resistance was 1500, 1800, and 2100 kN, the tunnel vault experienced the most severe lining damage. The damage at the foot of tunnel sidewall was also severe, although it was always less than the damage at the tunnel vault. The maximum damage for the three cases was 0.15, 0.13, and 0.09, with a declining trend. The damage at the foot of tunnel sidewall starts to exceed that at the

tunnel vault once the yielding resistance reaches 2400 kN. The maximum lining damage at the yielding resistance of 2400 kN is 0.12. The maximum damage value rises to 0.18 when the yielding resistance is 2700 kN, yet the damage at the foot of tunnel sidewall continues to be the highest, followed by the tunnel vault. The linings on both sides of the yielding member are damaged when the yielding resistance is 3000 kN. As a result, the most damaged area of the lining gradually shifts from the tunnel vault to the foot of tunnel sidewall as the yielding resistance increases. The maximum damage of lining under different yielding element resistance is shown in Fig. 20. The maximum damage shows a decreasing trend at first and then presents an upward trend with the resistance of the yielding member. The damage value is at its minimum and the yielding effect is at its maximum when the yielding resistance is 2100 kN.

Figure 21 shows the effect of yielding element resistance on principal stresses in the lining. The maximum compressive stress in the lining is 12.2, 13.8, 15.0, 14.1
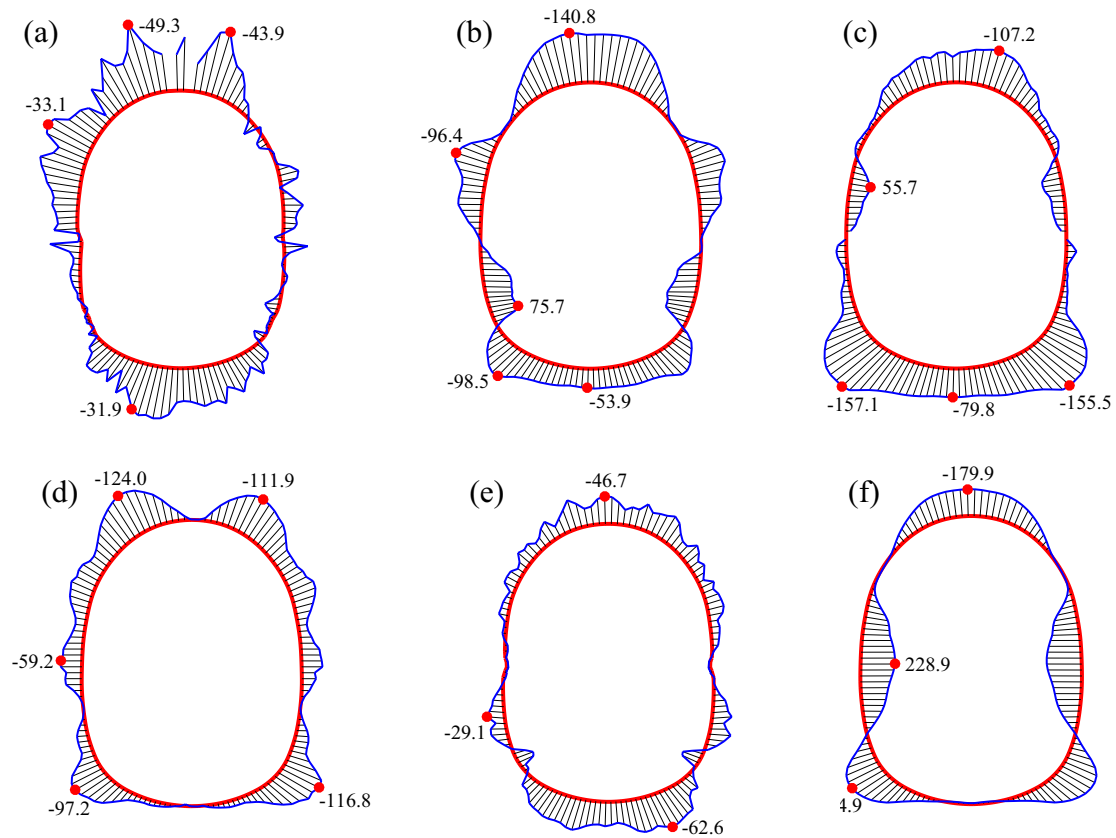
Fig. 17 Effect of yielding element position on bending moment (Unit: kN m). **a** Scheme A; **b** Scheme B; **c** Scheme C; **d** Scheme D; **e** Scheme E; **f** Scheme F

and 14.5 MPa for yielding resistances of 1500, 1800, 2100, 2400 and 2700 kN, respectively. The maximum compressive stress in the five cases does not exceed the load-carrying capacity of C25 concrete, demonstrating that the lining is in a satisfactory service condition. The maximum stress is just 5.8 MPa when the yielding resistance reaches 3000 kN and the stress is released when the lining fails. The stress in the lining is therefore less than

the concrete compressive strength when there is a reasonable yielding resistance.

Figure 22 shows the axial force distribution for various yielding resistances in the lining. When the yielding resistance is 3000 kN, the axial force of the lining is minimal, with a maximum axial force of 603.2 kN. The axial force near the yielding member is small in the remaining cases, but it is large at the vault and invert of the tunnel.

Fig. 18 Internal force of lining under different schemes. **a** Maximum axial force; **b** Maximum bending moment
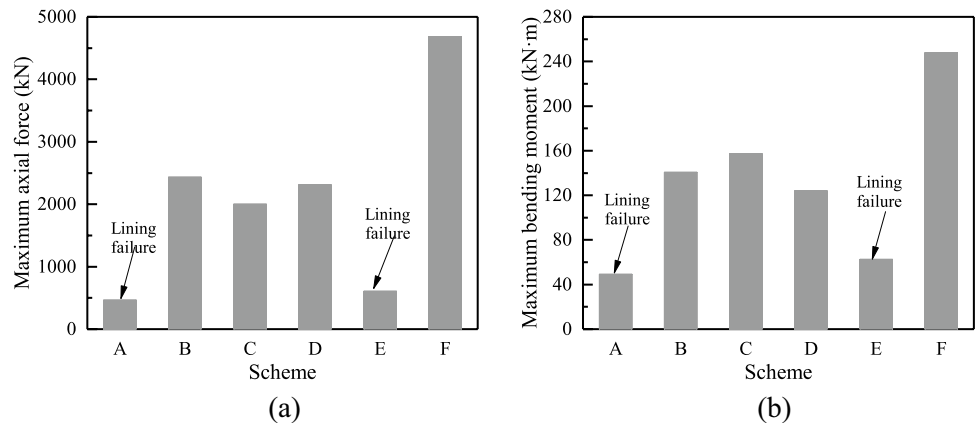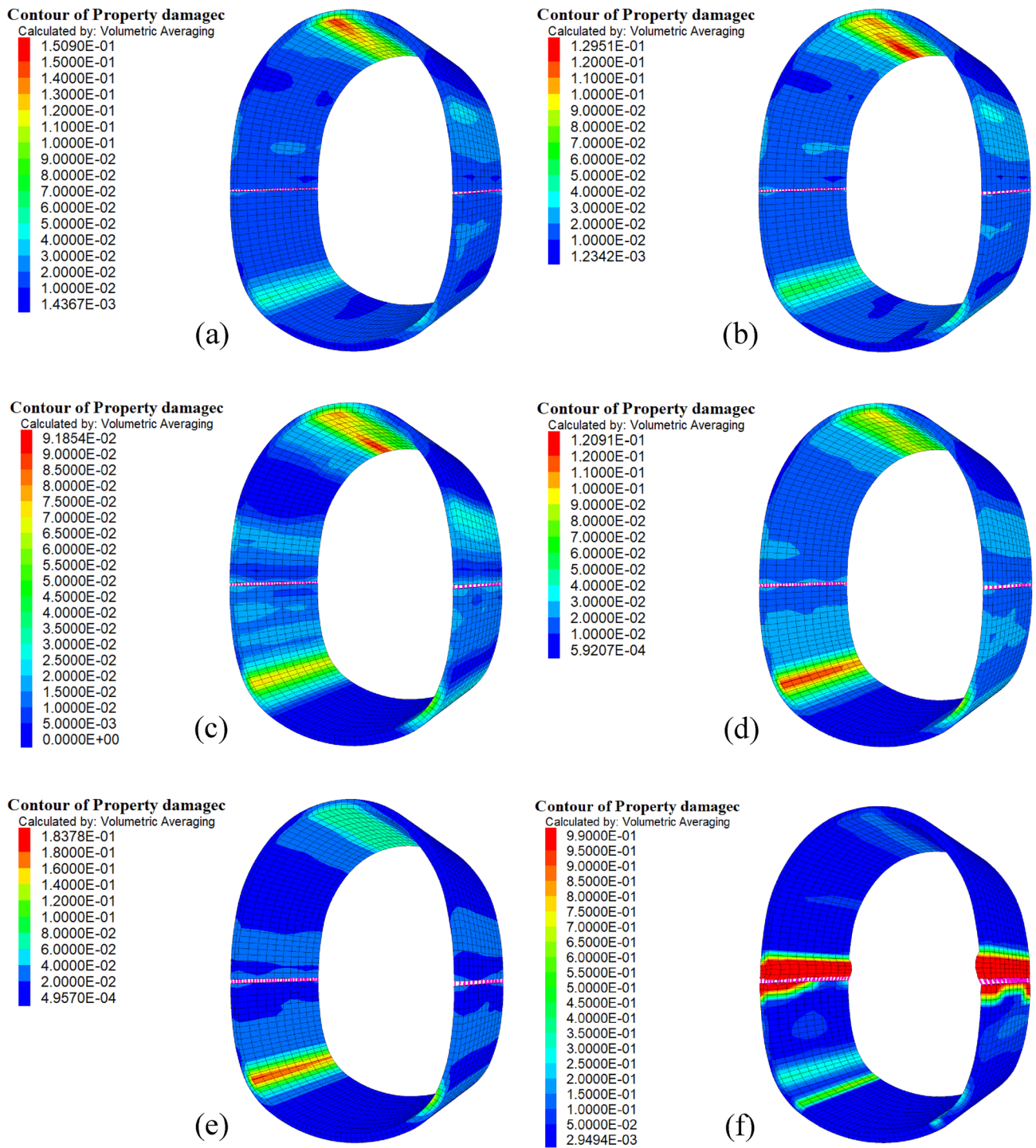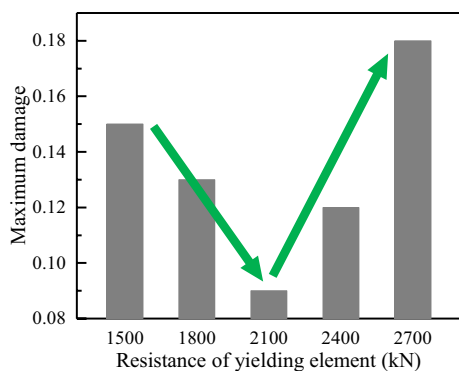
Fig. 19 Damage distribution of lining under different resistance of yielding element. **a** 1500 kN; **b** 1800 kN; **c** 2100 kN; **d** 2400 kN; **e** 2700 kN; **f** 3000 kN

When the yielding resistance is 1500 or 1800 kN, the axial force at the vault is less than that at the invert. When the yielding resistance reaches 2100, 2400, or 2700 kN, the axial force at the vault exceeds that at the invert. As a

Fig. 20 Maximum damage of lining under different resistance of yielding element

result, the yielding resistance affects the lining axial force distribution. The distribution of lining bending moments at various yielding resistances is shown in Fig. 23. Due to lining failure, the bending moment in the lining is minimal when the yielding resistance is 3000 kN. Except for the change in the value of the bending moment, the distribution features of the bending moment in the lining are the same in the other cases, that is, the bending moment is negative at the vault, the wall waist, and the invert, while it is positive in the other parts.

Figure 24 depicts the maximum internal force in the lining under different yielding resistances. It can be seen that the maximum lining axial force increases with increasing yielding resistance. When the yielding resistance reaches 3000 kN, the failure of the lining leads to a considerable decrease in the maximum axial force. On the premise that the lining is not damaged, the bending moment in the lining shows a slightly increasing trend as the yielding resistance goes up from 1500 to 1800 kN, which is followed by a significant drop till the lining is eventually failed as the resistance continues to increase. The maximum bending moments in the lining are approximately equal for yielding resistances of 1800 and 2100 kN. When the yielding resistance reaches 3000 kN, the maximum lining bending moment is significantly reduced due to the failure of the lining. The yielding resistance significantly affects the distribution of stress, damage, axial force, and bending moment of the lining. On the one hand, when the yielding resistance is inadequate, the surrounding rock pressure acting on the lining can be released constantly. If the surrounding rock is weak and broken, however, excessive release displacement will cause the surrounding rock to loosen, and the

surrounding rock pressure will be transformed from deformation pressure to loosening pressure. On the other hand, when the yielding resistance is too high, the pressure of the surrounding rock cannot be efficiently released, which invariably results in the lining failing. Therefore, the lining structure of the large-deformation tunnel has a reasonable yielding resistance, which can be determined according to the lining damage, axial force and bending moment. The reasonable yielding resistance in this investigation is 2100 kN.

5 Conclusion

This study performed a thorough investigation on the mechanical behavior of shotcrete lining with yielding support in a large-deformation tunnel. The highlight is that a concrete elastoplastic damage model and a numerical realization approach for the mechanical behavior of yielding support have been proposed. Based on the suggested model, the numerical analysis on the mechanical behaviors of shotcrete lining with yielding support has been performed, and the influences of key design parameters including the position and resistance of the yielding structure were revealed. The main conclusions are drawn as follows:

(1) The proposed elastic–plastic concrete damage model can describe the post-peak strain-softening behavior of concrete caused by damage under monotonic compression and tension. Furthermore, the employment of double-node beam elements and interface elements can accurately characterize the mechanical behavior of the yielding support structure. The elastoplastic damage model and yielding support simulation approach serve as the foundation for assessing the performance of shotcrete lining in large-deformation tunnels.

(2) When the resistance of the yielding member is constant, a reasonable arrangement position can prevent tunnel lining damage. In the tunnel dominated by horizontal deformation, the yielding structure arranged at the waist of the tunnel sidewall has the best yielding effect. The damage and maximum axial force are minimal, and the maximum bending moment is relatively large but lower than the maximum bending moment that the lining structure can bear.

(3) Assuming that the position of the yielding member stays the same, the maximum lining axial force rises with increasing yielding resistance, the maximum
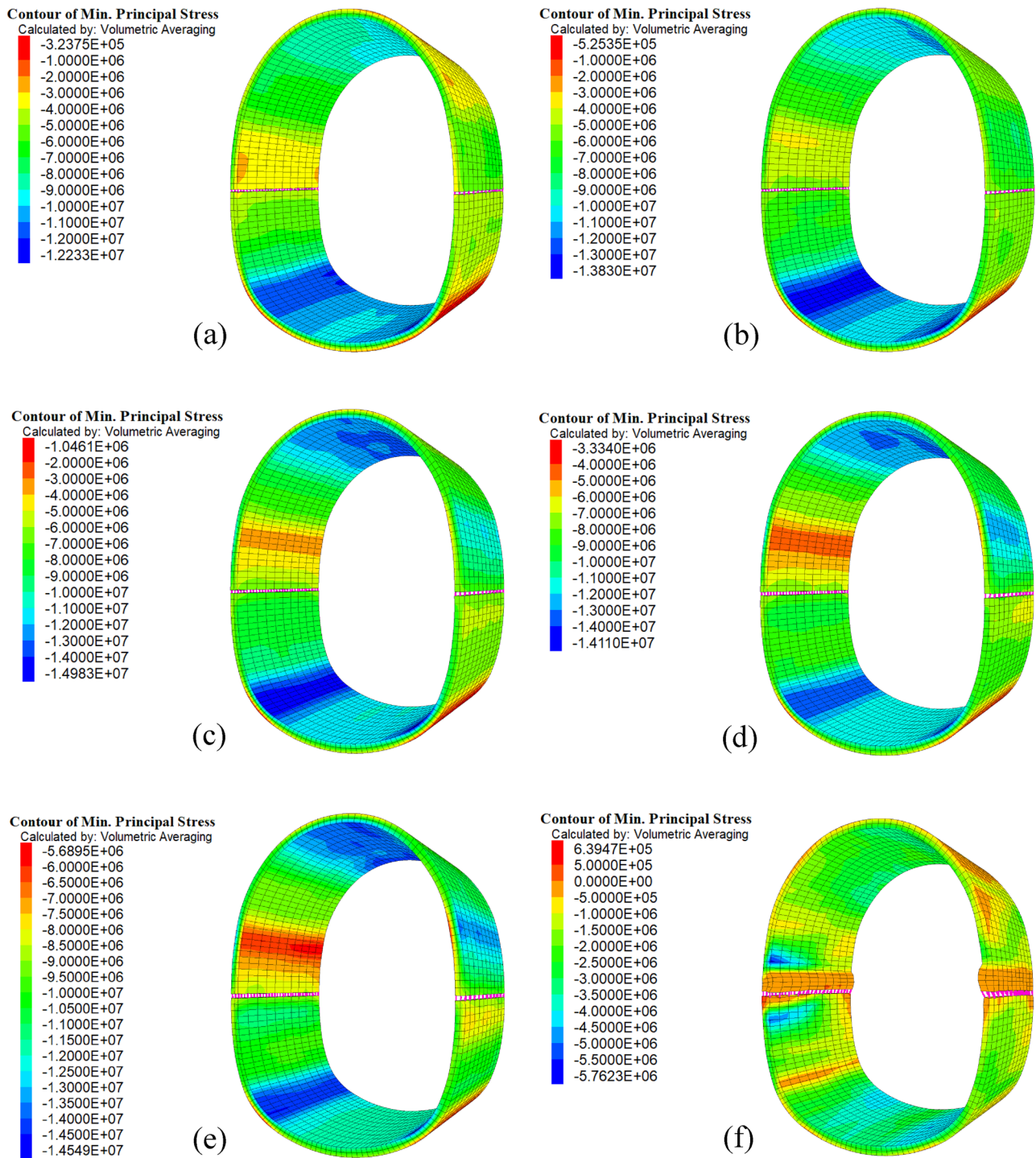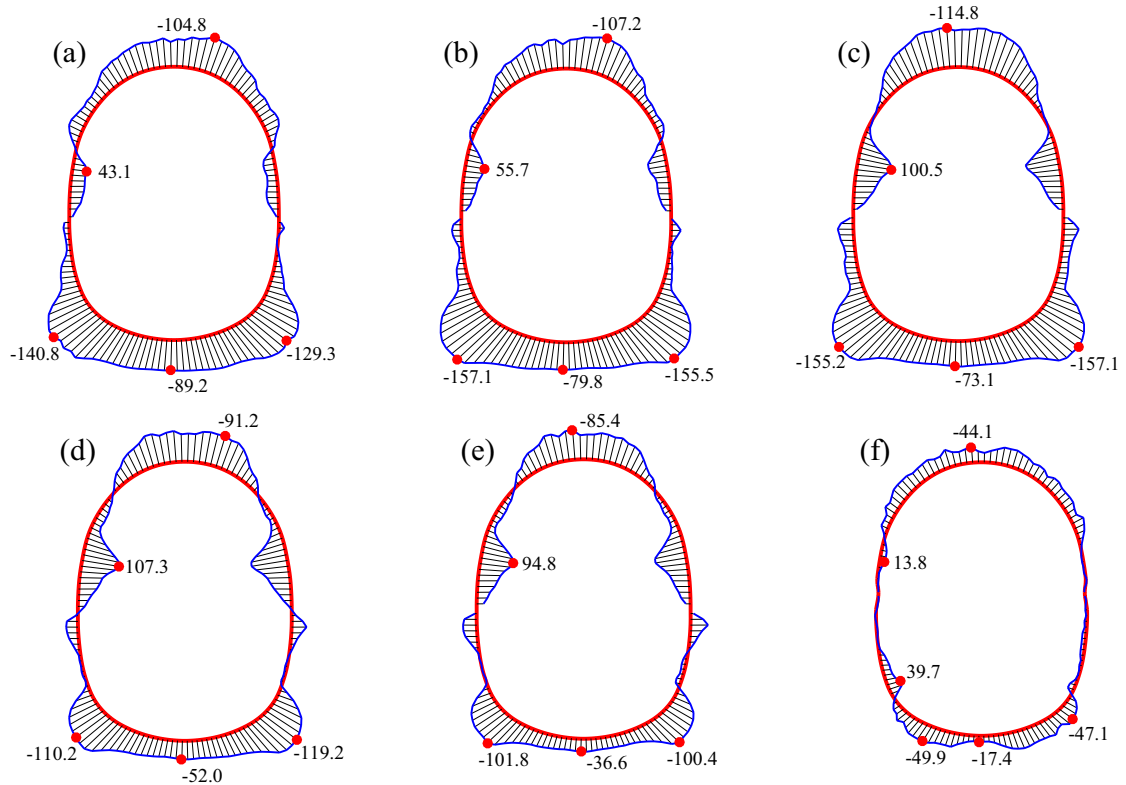
Fig. 21 The minimum principal stress distribution of lining under different yielding resistance (unit: Pa). **a** 1500 kN; **b** 1800 kN; **c** 2100 kN; **d** 2400 kN; **e** 2700 kN; **f** 3000 kN

bending moment shows an initially upward and subsequently downward trend as the yielding resistance rises, and the maximum damage shows a trend of first declining and then growing as the yielding resistance

rises. Additionally, this study found that the appropriate yielding resistance is 2100 kN.

(4) The position and resistance of the yielding member affect the distribution characteristics of damage, prin-
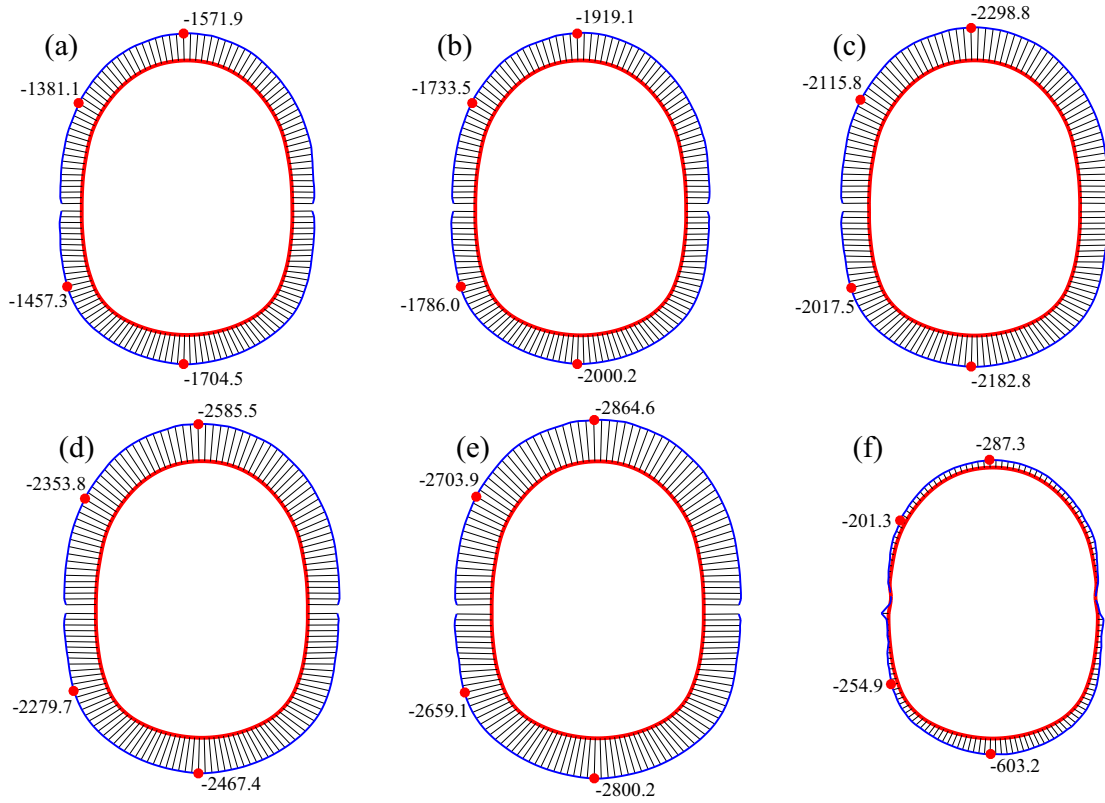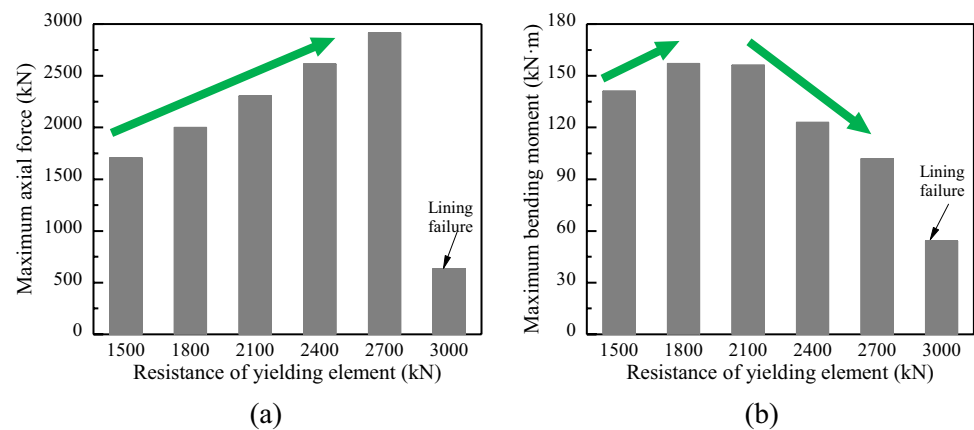
Fig. 22 Effect of yielding element resistance on axial force (Unit: kN). **a** 1500 kN; **b** 1800 kN; **c** 2100 kN; **d** 2400 kN; **e** 2700 kN; **f** 3000 kN

Fig. 23 Effect of yielding element resistance on bending moment (Unit: kN m). **a** 1500 kN; **b** 1800 kN; **c** 2100 kN; **d** 2400 kN; **e** 2700 kN; **f** 3000 kN

Fig. 24 Internal force of lining under different yielding resistance. **a** Maximum axial force; **b** Maximum bending moment

(a)

(b)

cipal stress, axial force and bending moment in shotcrete lining. The reasonable layout position and yielding resistance can effectively release surrounding rock pressure and transfer increasing axial force into the bending moment. As a result, the compressive stress in the lining is lower than the concrete compressive strength and lining damage is reduced or even eliminated.

Declarations

Conflict of interest The authors declare that they have no conflicts of interest.

References

Bai C, Xue Y, Qiu D, Yang W, Su M, Ma X (2021) Real-time updated risk assessment model for the large deformation of the soft rock tunnel. Int J Geomech 21:04020234. https://doi.org/10.1061/(ASCE)GM.1943-5622.0001887

Barla G, Bonini M, Debernardi D (2010) Time dependent deformations in squeezing tunnels. ISSMGE Int J Geoeng Case Hist 2:40–65

Chen H (2005) Constitutive equations for concrete and soil. China Architecture and Building Press, Beijing

Chen Z, He C, Yang W, Guo W, Li Z, Xu G (2020) Impacts of geological conditions on instability causes and mechanical behavior of large-scale tunnels: a case study from the Sichuan-Tibet highway, China. Bull Eng Geol Environ 79:3667–3688. https://doi.org/10.1007/s10064-020-01796-w

Cui G, Qi J, Wang D (2020) Research on large deformation control technology of tunnels in squeezing rock and its application. Sci Prog 103:0036850420923167. https://doi.org/10.1177/0036850420923167

Deng Y, Xie J, Li S (2020) Research and application of support resistant limiting dampers in the deep-buried large-section loess tunnel. Adv Civ Eng 2020:8841703. https://doi.org/10.1155/2020/8841703

Fabbri D (2004) The gotthard base tunnel: project overview. In: The 6th annual tunnelling 2004 conference, Sydney.

Guan B (1993) Introduction to tunnel mechanics. Southwest Jiaotong University publishing house, Chengdu

Guo Z (1999) Principles of reinforced concrete. Tsinghua University Press, Beijing

Guo Z, Shi X (2003) Reinforced concrete theory and analyse. Tsinghua University Press, Beijing

Hoek E, Brown ET (1997) Practical estimates of rock mass strength. Int J Rock Mech Min Sci 34:1165–1186. https://doi.org/10.1016/S1365-1609(97)80069-X

Itasca (2012) FLAC3D 5.0 manual. Itasca Consulting Group Minneapolis, Minneapolis

Kovári K (2005) Method and device for stabilizing a cavity excavated in underground construction. US Patent Appl. 20050191138

Kovári K (2009) Design methods with yielding support in squeezing and swelling rocks. In: World tunnel congress, Budapest, Hungary.

Lei S, Zhao W (2020) Study on the mechanism of circumferential yielding support for soft rock tunnel with large deformation. Rock Soil Mech 41:1039–1047

Ministry of Construction of the People's Republic of China (2002) Code for design of concrete structures (GB 50010–2002). China Architecture & Building Press, Beijing

National Railway Administration of China (2016) Code for design of railway tunnel vol TB 10003–2016. China Railway Publishing House Beijing, Beijing

Podjadtke R (2009) Development and application of stress controllers – system honeycomb—in modern tunneling. In: Proceedings of shotcrete for underground support XI

Qiu W, Wang G, Gong L, Shen Z, Li C, Dang J (2018) Research and application of resistance-limiting and energy-dissipating support in large deformation tunnel. Chin J Rock Mech Eng 37:1785–1795

Radončić N, Schubert W, Moritz B (2009) Ductile support design. Geomech Tunnel 2:561–577

Schubert W (1996) Dealing with squeezing conditions in Alpine tunnels. Rock Mech Rock Eng 29:145–153. https://doi.org/10.1007/BF01032651

Tao Z (1987) Rockburst and its discrimination at high stress zone. People Yangtze River 5:25–33

Tao Z, Zhao F, Wang H, Zhang H, Peng Y (2017) Innovative constant resistance large deformation bolt for rock support in high stressed rock mass. Arab J Geosci 10:341. https://doi.org/10.1007/s12517-017-3127-5

Thut A, Naterop D, Steiner P, Stolz M (2006) Tunnelling in squeezing rock-yielding elements and face control. In: 8th international

conference on tunnel construction and underground structures, Ljubljana, Ljubljana, Slovenia. pp 221–241

Tian H, Chen W, Yang D, Wu G, Tan X (2016) Numerical analysis on the interaction of shotcrete liner with rock for yielding supports. Tunnel Undergr Sp Technol 54:20–28. https://doi.org/10.1016/j.tust.2016.01.025

Tian HM, Chen WZ, Tan XJ, Yang DS, Wu GJ, Yu JX (2018) Numerical investigation of the influence of the yield stress of the yielding element on the behaviour of the shotcrete liner for yielding support. Tunnel Undergr Sp Technol 73:179–186. https://doi.org/10.1016/j.tust.2017.12.019

Wang B, He M, Qiao Y (2021) Resistance behavior of Constant-Resistance-Large-Deformation bolt considering surrounding rock pressure. Int J Rock Mech Min Sci 137:104511. https://doi.org/10.1016/j.ijrmms.2020.104511

Wang B, Wang J, Wu D, Zhao Y, Zhang B, Li Z (2016) Study on application of yielding supporting system for large-deformation in soft rock highway tunnel. J Railw Sci Eng 13:1985–1993. https://doi.org/10.19713/j.cnki.43-1423/u.2016.10.016

Wu G, Chen W, Tian H, Jia S, Yang J, Tan X (2018) Numerical evaluation of a yielding tunnel lining support system used in limiting large deformation in squeezing rock. Environ Earth Sci 77:439. https://doi.org/10.1007/s12665-018-7614-0

Wu K, Shao Z, Qin S, Li B (2020) Determination of deformation mechanism and countermeasures in silty clay tunnel. J Perform Constr Facil 34:04019095. https://doi.org/10.1061/(ASCE)CF.1943-5509.0001381

Wu K, Shao Z, Sharifzadeh M, Hong S, Qin S (2021) Analytical computation of support characteristic curve for circumferential yielding lining in tunnel design. J Rock Mech Geotech Eng. https://doi.org/10.1016/j.jrmge.2021.06.016

Xiao P, Li D, Zhao G, Liu H (2021) New criterion for the spalling failure of deep rock engineering based on energy release. Int J Rock Mech Min Sci 148:104943. https://doi.org/10.1016/j.ijrmms.2021.104943

Xu G, Gutierrez M (2021) Study on the damage evolution in secondary tunnel lining under the combined actions of corrosion degradation of preliminary support and creep deformation of surrounding rock. Transp Geotech 27:100501. https://doi.org/10.1016/j.trgeo.2020.100501

Zhang H, Huang YJ, Yang ZJ, Xu SL, Chen XW (2018) A discrete-continuum coupled finite element modelling approach for fibre reinforced concrete. Cem Concr Res 106:130–143. https://doi.org/10.1016/j.cemconres.2018.01.010

Zhang Y, Zhao G, Wei X, Li H (2021) A multifrequency ultrasonic approach to extracting static modulus and damage characteristics of rock. Int J Rock Mech Min Sci 148:104925. https://doi.org/10.1016/j.ijrmms.2021.104925